JOURNAL OF GEOPHYSICAL RESEARCH, VOL. 98, NO. D10, PAGES 18,367–18,376, OCTOBER 20, 1993

Atmosphere-Snow Transfer Function for H_2O_2: Microphysical Considerations

MARTHA H. CONKLIN

Department of Hydrology and Water Resources, The University of Arizona, Tucson, Arizona

ANDREAS SIGG AND ALBRECHT NEFTEL

Physics Institute, University of Bern, Bern, Switzerland

ROGER C. BALES

Department of Hydrology and Water Resources, The University of Arizona, Tucson, Arizona

H_2O_2 analyses of polar ice cores show an increase in concentration from 200 years to the present. In order to quantitatively relate the observed trend in the ice to atmospheric levels, the atmosphere-snow transfer behavior and postdepositional changes must be known. Atmosphere-snow transfer was studied by investigating uptake and release of H_2O_2 in a series of laboratory column experiments in the temperature range -3°C to -45°C. Experiments consisted of passing H_2O_2-containing air through a column packed with 200-μm diameter ice spheres and measuring the change in gas phase H_2O_2 concentration with time. The uptake of H_2O_2 was a slow process requiring several hours to reach equilibrium. Uptake involved incorporation of H_2O_2 into the bulk ice as well as surface accumulation. The amount of H_2O_2 taken up by the ice was greater at the lower temperatures. The sticking coefficient for H_2O_2 on ice in the same experiments was estimated to be of the order of 0.02 to 0.5. Release of H_2O_2 from the ice occurred upon passing H_2O_2-free air through the packed columns, with the time scale for degassing similar to that for uptake. These results suggest that systematic losses of H_2O_2 from polar snow could occur under similar conditions, when atmospheric concentrations of H_2O_2 are low, that is, in the winter.

INTRODUCTION

Analysis of Greenland ice cores has demonstrated that H_2O_2 is one of the most abundant trace species for locations that have mean annual temperatures below -15°C. Relating the measured ice concentrations to past atmospheric concentrations, however, cannot be achieved with great confidence until the transfer behavior between the atmosphere and snow/firn is understood. A large set of snow and ice measurements are available for Greenland [*Sigg and Neftel*, 1991, 1988], and Antarctica [*Neftel et al.*, 1984, 1986]. The observations show that postdepositional processes change H_2O_2 concentrations as fresh snow metamorphoses, becomes firn, and eventually becomes ice [*Sigg et al.*, 1992*b*]. In samples from sites with mean annual temperatures above -15°C, an almost complete loss of H_2O_2 in the upper layers was measured. Estimated time scales for this process range from months to years. The same observations of losses with time have been made in seasonal snowpacks in the Sierra Nevada [*Gunz and Hoffmann*, 1990] and in the Alps [*Sigg et al.*, 1987].

A measurement on a sample from a snowpack or from an ice core yields a mean value over a specific depth interval ($\bar{C}_i$), which corresponds to an integration over time. The time and depth resolutions are functions of the mixing processes that take place after the snow is deposited: (1) redistribution of snow at the surface (wind blowing), (2) evaporation and recondensation, and (3) transport in the snowpack. The relative importance of these processes has to be determined to define a transfer function for H_2O_2 accumulation in the ice core. In this paper, we investigate the third process.

In addition to local variations, differences in amounts of H_2O_2 accumulation are observed. The mean H_2O_2 concentration in the ice is higher at Siple or Byrd than at South Pole station [*Neftel et al.*, 1984; *Sigg and Neftel*, 1991]. A systematic loss from low-accumulation cores from cold locations in Antarctica is the most probable explanation. In order to understand these loss processes and postdepositional changes, the processes need to be quantified and transfer functions developed.

Conceptually, a transfer function $\bar{C}_i/\bar{C}_a$ implies averaging over time periods of at least several days to weeks. $\bar{C}_a$ is a time and spatial average concentration in the atmosphere. The transfer function can depend on processes that occur on the microscale (ice grain surfaces) to macroscale (kilometers). We report a series of laboratory column experiments designed to investigate the temperature dependence (-3°C to -45°C) of the uptake and release of H_2O_2 on snow. These experiments were designed to determine the time scales of processes that occur on the microscale. Specific questions that were investigated are (1) is the uptake and release of H_2O_2 reversible, (2) what is the temperature dependence, (3) what is the dependence of uptake on gas phase concentrations, (4) what are the time scales of these processes, (5) is the sticking coefficient of H_2O_2 on ice less than for H_2O on ice, and (6) what is the importance of surface versus bulk ice processes.

CONCEPTUAL MODEL

One can consider the exchange of H_2O_2 between air and ice to be a three-step process involving physical adsorption

Paper number 93JD01194.
0148-0227/93/93JD-01194$05.00.

of H_2O_2 at the interface, followed by either (1) incorporation of the H_2O_2 into the surface region where water molecules are also being deposited/exchanged (codeposition) or (2) partitioning of H_2O_2 into an aqueous surface region in accord with Henry's law of equilibrium. The third step is incorporation of H_2O_2 into the bulk ice. These steps are illustrated in Figure 1 with C_a, C_{ad}, C_s and C_b representing H_2O_2 concentrations in the air, air-ice interface, surface-disordered layer and bulk ice, respectively. The rate limiting step could involve transfer between any of these phases. It is our hypothesis that at short time scales the second step should control the rate and extent of uptake. At longer time scales, diffusion into and out of the bulk ice will be important.

For air being advected through ice in one dimension, that is, a column experiment, the change in H_2O_2 concentrations in air (C_a) and ice (C_i) (mol m^{-3}) equals the changes due to dispersion and advection

$$\theta_a \frac{\partial C_a}{\partial t} + \theta_i \frac{\partial C_i}{\partial t} = \theta_a D_a \frac{\partial^2 C_a}{\partial x^2} - \theta_a u_a \frac{\partial C_a}{\partial x} \quad (1)$$

where θ_a and θ_i are the respective volume fractions of air and ice; D_a is the dispersion coefficient in the flowing air (m^2 s^{-1}); and u_a is the average air velocity in the column voids (m s^{-1}). In this equation dispersion refers to the sum of mechanical dispersion and diffusion. Mechanical dispersion, the spreading out of the front due to pathways through the porous media, dominates; it is relatively insensitive to temperature. The second equation needed to solve for C_a and C_i comes from a general expression for slow air-ice transfer

$$\theta_i \frac{\partial C_i}{\partial t} = \theta_a k_f C_a - \theta_i k_b C_i = \theta_a k_f \left[C_a - \frac{C_i}{K_D} \right] \quad (2)$$

where k_f and k_b are pseudo-first-order rate coefficients, or mass transfer coefficients (s^{-1}), and K_D is the air-to-ice equilibrium partition coefficient (cm_a^3 cm_i^{-3}). In terms of the conceptual model of Figure 1, k_f is an overall mass transfer coefficient, and K_D is an overall partition coefficient representing the ratio between ice and air concentrations, C_a/C_i, which is equal to $k_f \theta_a / k_b \theta_i$. It should be noted that C_i represents the sum of ice surface and bulk concentrations. Depending on the rate controlling steps, the magnitude of k_f and k_b can be determined by any of three reversible processes shown in Figure 1.

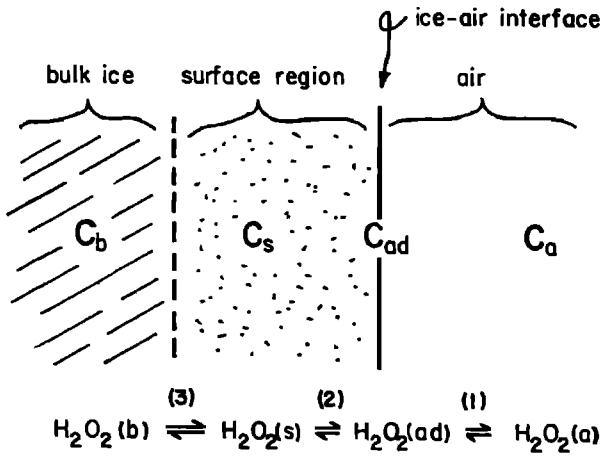

Fig. 1. Conceptual model of partitioning at ice-air interface. Any of the three reversible reactions illustrated: (1) adsorption, (2) partitioning to surface disordered region, and (3) partitioning to bulk ice, can be rate limiting. In the presence of liquid water, equilibrium between C_a and C_s would be expressed by Henry's law. C_a can also reflect codeposition of H_2O_2 and H_2O.

Initial and boundary conditions in the column are

$$C_a(x, 0) = 0 \quad (3)$$

$$\frac{\partial C_a(\infty, t)}{\partial x} = 0 \quad (4)$$

$$u_a C_a(0, t) - D_a \frac{\partial C_a(0, t)}{\partial x} = u_a C_0 \quad (5)$$

where C_0 is the concentration at the column inlet.

Defining the dimensionless variables $C_1 = C_a/C_0$, $C_2 = C_i/K_D C_0$, $X = x/L$, and $T = t u_a/L$, where L is the column length; and substituting these into equations (1) and (2) yields the dimensionless transport equations

$$\beta R \frac{\partial C_1}{\partial T} + (1 - \beta) R \frac{\partial C_2}{\partial T} = \frac{1}{P} \frac{\partial^2 C_1}{\partial X^2} - \frac{\partial C_1}{\partial X} \quad (6)$$

$$(1 - \beta) R \frac{\partial C_2}{\partial T} = \omega (C_1 - C_2) \quad (7)$$

where $R = 1 + (\theta_i/\theta_a) K_D$, $\beta = 1/R$, $P = u_a L/D_a$ and $\omega = k_f L/u_a$.

Initial and boundary conditions in equations (3) – (5) are then

$$C_1(X, 0) = 0 \quad (8)$$

$$\frac{\partial C_1(\infty, T)}{\partial X} = 0 \quad (9)$$

$$C_1(0, T) - \frac{1}{P} \frac{\partial C_1(0, T)}{\partial X} = 1 \quad (10)$$

Analytical solutions are available for equations of this form [e.g., *Van Genuchten and Wierenga*, 1976]. The parameter R, a retardation factor or retention volume, gives the number of pore volumes of air for which H_2O_2 was retained in the column at equilibrium. For a conservative tracer $R = 1$; $R > 1$ for any species that sorbs to the ice. Dimensionless time T expresses the pore volumes of air passed through the column. The parameter ω is a Damkohler number and is the ratio of the column residence time (L/u_a) to the time scale for mass transfer (k_f^{-1}). If ω is large (≥ 100), mass transfer is fast relative to the column residence time and equilibrium conditions should prevail; we refer to this case as an equilibrium model. If ω is small, mass transfer is slow and nonequilibrium conditions should prevail; we refer to this case as a first-order model. The Peclet number P reflects the amount of dispersion in the column. The parameter k_f represents an overall mass transfer coefficient for a first-order process. The rate-limiting step for this process could be the rate H_2O_2 molecules are deposited to the surface or slow diffusion into the bulk ice, that is, processes 2 and 3 in Figure 1, respectively. Both sets of equations are developed and used to help interpret the experimental data.

The rate at which H_2O_2 molecules are deposited on ice in the column can be estimated using a single-collector approach [e.g., *Friedlander*, 1958]. The single-collector removal efficiency η is defined as

$$\eta = \frac{\textit{Rate at which molecules strike a collector}}{\textit{Rate at which molecules approach a collector}} \quad (11)$$

Molecules are transported from the moving fluid to the ice

surface by Brownian diffusion, with η given as $\eta = 4.04\, A_s^{1/3}\, Pe^{-2/3}$, where Pe is a diffusion Peclet number, equal to $u_a\, d/D_0$ [*Levich*, 1962], where D_0 is the H_2O_2 diffusion coefficient in air, d is the diameter of the ice spheres and A_s accounts for the effect of adjacent collectors on the flow around a single collector

$$A_s = \frac{1-\varepsilon^5}{1-1.5\varepsilon+1.5\varepsilon^5-\varepsilon^6} \tag{12}$$

where $\varepsilon = \theta_a^{1/3}$ [*Happel*, 1958]. The factor A_s is necessary to relate the rate of diffusion to a single spherical collector (η) to that in an assembly of packed spheres.

The single-collector removal efficiency η can be related to the mass transfer coefficient k_f, using the sticking efficiency α, (analogous to a mass accommodation coefficient for gases striking liquids) is defined as

$$\alpha = \frac{\textit{Rate at which molecules stick to a collector}}{\textit{Rate at which molecules strike a collector}} \tag{13}$$

H_2O_2 molecules are removed from a unit volume of air at the rate $k_f C_a$ and thus are removed by (stick to) a single collector at the rate $k_f\, C_a \left[\pi\theta_a d^3/(6\theta_i)\right]$ where the quantity in parentheses is the volume of air associated with a single, spherical collector of diameter d. The rate at which impurity molecules approach this volume is $\theta_a u_a C_a \left[\pi d^2/4\right]$, giving

$$\eta\,\alpha = \frac{2}{3}\,\frac{k_f d}{u_a}\,\frac{1}{\theta_i} \tag{14}$$

Rearranging, gives

$$k_f = \frac{3}{2}\,\frac{u_a\theta_i}{d}\eta\alpha \tag{15}$$

The unknown parameter α is related to ω, which can be estimated from experimental data. Combining equation (15) and the definition of ω gives

$$\alpha = \frac{2}{3}\,\frac{d\,\omega}{\theta_i L}\,\frac{1}{\eta} \tag{16}$$

If the rate-limiting process is assumed to be the uptake of H_2O_2 molecules by the surface, this equation gives a value for the sticking coefficient. If, however, the rate-limiting process is a combination of both diffusion into the ice and incorporation into the surface layer, this model will underestimate the sticking coefficient.

An alternative interpretation of the dominant rate limiting process is to consider diffusion into the bulk ice. To do this analysis, one needs to consider the geometry of the system. Assuming spherical particles, the average ice-phase concentration (C_i), is determined by integration

$$C_i = \frac{3}{a^3}\int_0^a r^2\, C_r\, dr \tag{17}$$

where C_r is the local H_2O_2 concentration at any point in the ice sphere, assumed to be radially homogeneous; and a is the average sphere radius (10^{-4} m). H_2O_2 transport in an ice sphere is governed by the spherical diffusion equation

$$\frac{\partial C_r}{\partial t} = \frac{D_i}{r^2}\,\frac{\partial}{\partial r}\left[r^2\,\frac{\partial C_r}{\partial r}\right] \tag{18}$$

where D_i is the H_2O_2 diffusion coefficient in the ice.

Boundary conditions for diffusion in the ice spheres are assumed to be

$$C_r(x,a,t) = K_D\, C_a\,(x,t) \tag{19}$$

$$\frac{\partial\, C_r(x,0,t)}{\partial r} = 0 \tag{20}$$

Setting $\xi = r/a$ and $C_3 = C_r/(D_D\, C_0)$, equation (18) becomes

$$\frac{\partial C_3}{\partial T} = \gamma\frac{1}{\xi^2}\,\frac{\partial}{\partial\xi}\left[\xi^2\frac{\partial C_3}{\partial\xi}\right] \tag{21}$$

where $\gamma = L\, D_i/(u_a\, a^2)$. Boundary conditions are then

$$C_3(X,1,T) = C_1(X,T) \tag{22}$$

$$\frac{\partial C_3(X,0,T)}{\partial T} = 0 \tag{23}$$

Equation (17) becomes

$$C_2 = 3\int_0^1 \xi^2\, C_3\, d\,\xi \tag{24}$$

The parameter γ in the spherical-diffusion equation is proportional to ω estimated from the simple mass transfer model [*Van Genuchten*, 1985]. For spherical geometry, $\gamma = 0.441\omega/(R-1)$. Thus, $D_i = (0.0441\omega/(R-1))\,(u_a\, a^2/L)$. The constant, 0.441, is a geometry-based shape factor for spherical aggregates that is used to relate γ to the mass transfer coefficient determined from the first-order model. For the case where diffusion into ice is the rate-limiting step, D_i can be determined from parameter estimates for ω and R.

METHODS

A series of eight continuous-flow column experiments were carried out to examine the uptake of H_2O_2 onto ice spheres (200-μm diameter) at temperatures from -3° to -45°C. Ice spheres of deionized water were produced using the technique of *Sommerfeld and Freeman* [1988]. The frozen ice spheres were packed into glass columns (5 cm or 2.5 cm length, 0.4 cm diameter) that had the inside precoated with ice and were subsequently sintered for time intervals of 4 to 36 hours. During the experiments the ice columns were placed into a constant-temperature oven (Despatch model 926) and a constant concentration of H_2O_2 advected through the column. A block diagram of the apparatus is shown in Figure 2, with experimental conditions listed in Table 1.

The column-outlet H_2O_2 concentration was measured using a continuous-flow detector. The sorption limbs of the breakthrough curves were obtained by saturating the column with H_2O_2, with saturation defined as the point when the H_2O_2 concentration of the column outflowequaled that of the column inflow. In three of the experiments H_2O_2-free air was passed through the column in the later portion of the experiment to determine the reversibility of H_2O_2 uptake; this portion of the breakthrough curve is referred to as the desorption limb.

The complete description of the H_2O_2 calibration gas source and H_2O_2 detector [*Sigg et al.*, 1992*a*] is not readily available, so a brief description follows. The constant concentration of H_2O_2 was produced by passing dry, H_2O_2-free air (zero air) through a 50-cm long microporous polypropylene tube (Accurel 1.8 mm ID by 2.6 mm OD, Enka AG, Wuppertal) that was immersed in a constant-temperature (0°C) 0.01

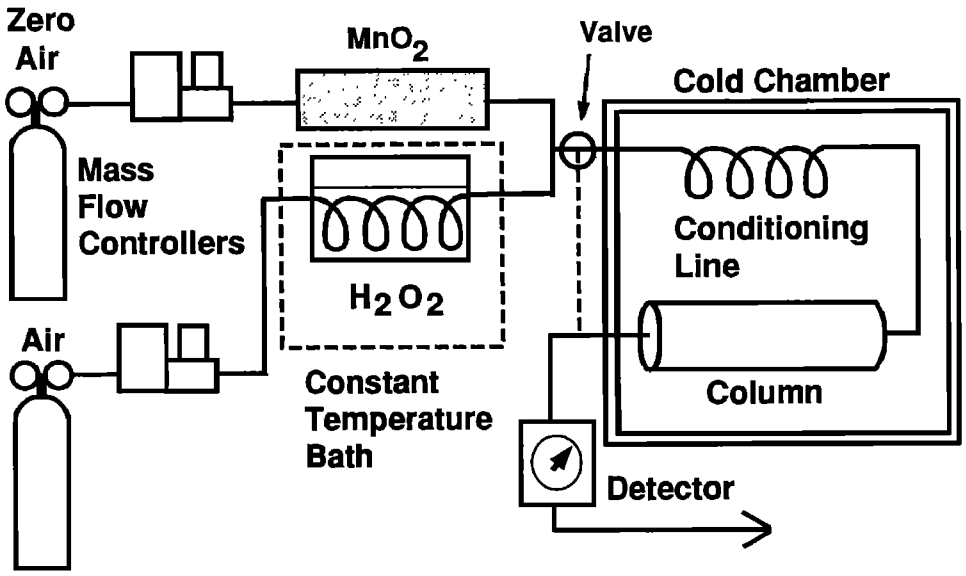

Fig. 2. Experimental apparatus.

TABLE 1. Experimental Conditions and Results

Exp	Temperature, °C	C_0 ppbv	Column Length, m	θ_i	u_a ms^{-1}	Duration of H_2O_2 Feed, s	H_2O_2 Uptake, nmoles, % of Feed: Bulk Ice[a]	H_2O_2 Uptake, nmoles, % of Feed: Breakthrough Curve[b]	H_2O_2 Degassed, [c] %
1	-29	6.2	0.050	0.49	2.2	4.9×10^4	36 (17)	61 (28)	...
2	-12.5	39.0	0.050	0.49	2.2	9×10^3	47 (18)	65 (25)	...
3	-3	90.8	0.050	0.49	2.2	7.2×10^3	75 (15)	134 (28)	...
4	-45	1.17	0.025	0.64	2.8	4.68×10^4	9 (24)	23 (58)	...
5	-9.5	45.8	0.050	0.60	1.98	6.6×10^3	59 (35)	77 (45)	...
6	-3	93.5	0.050	0.40	2.0	7.8×10^3	22[d]	189 (35)	47
7	-30	67.4	0.025	0.54	2.0	3.92×10^4	–[d]	325 (16)	33
8	-45	13.5	0.025	0.61	2.6	5.7×10^4	–[d]	391 (71)	10

[a]From melting and analysis of ice at the end of experiment.
[b]From are above breakthrough curve (see Figure 3).
[c]Based on breakthrough curves.
[d]These samples were degassed before melting.

M H_2O_2 solution. Zero air was generated from dry cylinder air by scrubbing out H_2O_2 and organic peroxides using two columns (5 cm long, 1 cm ID) filled with granular manganese dioxide and activated carbon. The detector required a flow rate of 1 L min^{-1}, so additional zero air was combined with the H_2O_2-containing stream; proportions were set as to give air that was slightly below the calculated dew point of the experimental temperature. To prevent condensation, accurate flow control was required; mass flow controllers (Sierra Instruments) were used. All flow rates were corrected for the 0.16 atm back pressure introduced by the ice column. This method resulted in a range of H_2O_2 concentrations for the temperatures used (1.17 to 93.5 ppbv). The H_2O_2 air stream concentration was calibrated at the beginning and end of each experiment by comparing the detector response to liquid H_2O_2 standards. This H_2O_2 air stream was used for inflow into the column.

To check for detector drift, the detector cycles between measuring sample air for 20 s and zero air for 100 s. To check the detector response, the same cycle was repeated with the constant H_2O_2/air mixture (i.e., calibration gas for 20 s and zero air for 100 s). In all cases, no detectable drift was observed.

The H_2O_2 detector was based on the transfer of gaseous H_2O_2 to a scrubber liquid followed by enzymatic fluorometric detection in the aqueous phase. The principle of operation is described by *Dasgupta et al.* [1988]. The gas phase system consists of three lines: sample, zero, and calibration. The sample enters a straight acrylic glass tube (40 cm × 0.67 cm ID), inside this tube is a 30 cm perfluorinated ion exchange membrane tubing (Nafion 020, Perma Pure Products), which is the scrubber membrane and has H_2O flowing through it at 0.1 mL min^{-1} [*Zhang et al.*, 1992]. The collection efficiency of this Nafion scrubber at 1.0 L min^{-1} is of the order of 70% and has a linear response to the concentration range [*Zhang et al.*, 1992]. After the scrubber, reagent solution is added at 0.05 mL min^{-1} (0.01 M 4-ethylphenol, 0.05 M phosphate buffer at pH 6 and 1 unit mL^{-1} peroxidase). Between the reagent addition and the detector, the pH is raised to 9.0 by passing the solution through a 1-cm length of Nafion tubing suspended over a 25% NH_4OH solution [*Hwang and Dasgupta*, 1986].

The fluorescence detector consists of a cadmium lamp (Hamamatsu L 2264), interference filters (excitation 326 ±5 nm lot 326FS10-25; emission 400 nm ±20 nm lot 400FS40-25) and a photomultiplier tube (Hamamatsu R268) in a high-voltage power supply/signal amplifier housing (Seitner ME 1030 FK-E). The fluorescence cell is a fused silica cylinder tube (2 mm ID, 4 mm OD, 5 mm length).

To avoid any ice deposition, the relative humidity was

kept from 80 to 95%; at the lower humidities some erosion could occur within the first centimeter. At higher humidities, deposition would clog the column. Visual inspection and column back pressure measurements showed this was minimal. The surface area of the column packing may have changed slightly during the longer experiments, due to the short sintering time. However, the size of the ice spheres was chosen to minimize that effect [*Perla*, 1978]. The surface-to-volume ratio, measured in similarly packed columns using stereology [*Conklin et al.*, 1993] was determined to be 15 $mm^2\ mm^{-3}$ for the sintered ice spheres, that is, conditions at the end of an experiment. For unsintered 200-μm diameter spheres, the surface-to-volume ratio is 30 $mm^2\ mm^{-3}$.

RESULTS

There was significant H_2O_2 uptake in each experiment. Breakthrough curves exhibited a slow rise in column-outlet concentration (C), from $C_a/C_0 = 0$ to $C_a/C_0 = 1.0$ (Figure 3). The fraction of H_2O_2 taken up by the ice was greater at lower temperatures (Table 1), as was the time required for concentrations in the air and ice to reach equilibrium. These results indicated H_2O_2 uptake increases with decreasing temperature. Experiments at -3° to -30°C reached $C_a/C_0 \approx 1$ after 1.5 to 8 hours. Air had a residence time of about 0.023 s in the 2.5-cm column, so 2.3×10^5 to 1.25×10^6 pore volumes of gas passed through the column before equilibrium was reached. At -45°C, C_a/C_0 was only 0.4-0.5 after 14-16 hours; that is, uptake was greater at -45°C than at higher temperatures.

Degassing at -3° and -30°C resulted in a comparable time for C_a/C_0 to drop to near 0 as for C_a/C_0 to reach 1 in the uptake portion of the experiment. Only 47 and 33% of the H_2O_2 taken up was degassed at the two temperatures, respectively. Degassing was slow in experiment 8 (-45°C), and was not carried to completion. These results suggest that the uptake of H_2O_2 was reversible.

There was no apparent influence of gas phase concentration on either extent or rate of H_2O_2 uptake. For example, experiment 7 (-30°C) had a C_0 10 times that in experiment 1 (-29°C), but the breakthrough curves were quite similar. The small differences in breakthrough curves for experiments 3 versus 6 and experiments 4 versus 8 are thought to be due to factors other than concentration, as discussed below.

As H_2O_2 uptake in experiments 4 and 8 failed to reach equilibrium, the equilibrium uptake was estimated with the aid of the advection-dispersion model that describes H_2O_2 transport through the column. The same model was used to estimate the rates of H_2O_2 uptake and release.

A nonlinear-least-squares algorithm [*Van Genuchten*, 1981] was used to estimate the model parameters (retardation factor (R), Peclet number (P), and Damkohler number (ω)) from the experimental data, with results presented in Table 2. In order to estimate ω, the dispersion Peclet number must be known independently of the experimental data to be fitted. This is because the values of both parameters can be adjusted to reproduce the shape of the curve as it approaches equilibrium. To estimate P, we first fit the curves for temperatures $\geq$ -30°C to an equilibrium model ($\omega \geq 100$). The equilibrium model provided a good fit to the data, but estimated Peclet numbers were quite low. The fitted values of P ranged from 0.77 (experiment 1) to 14 (experiment 6) (Table 2). This gave a lower limit on P, since only the dispersion term can account for the slow approach to C_a/C_0

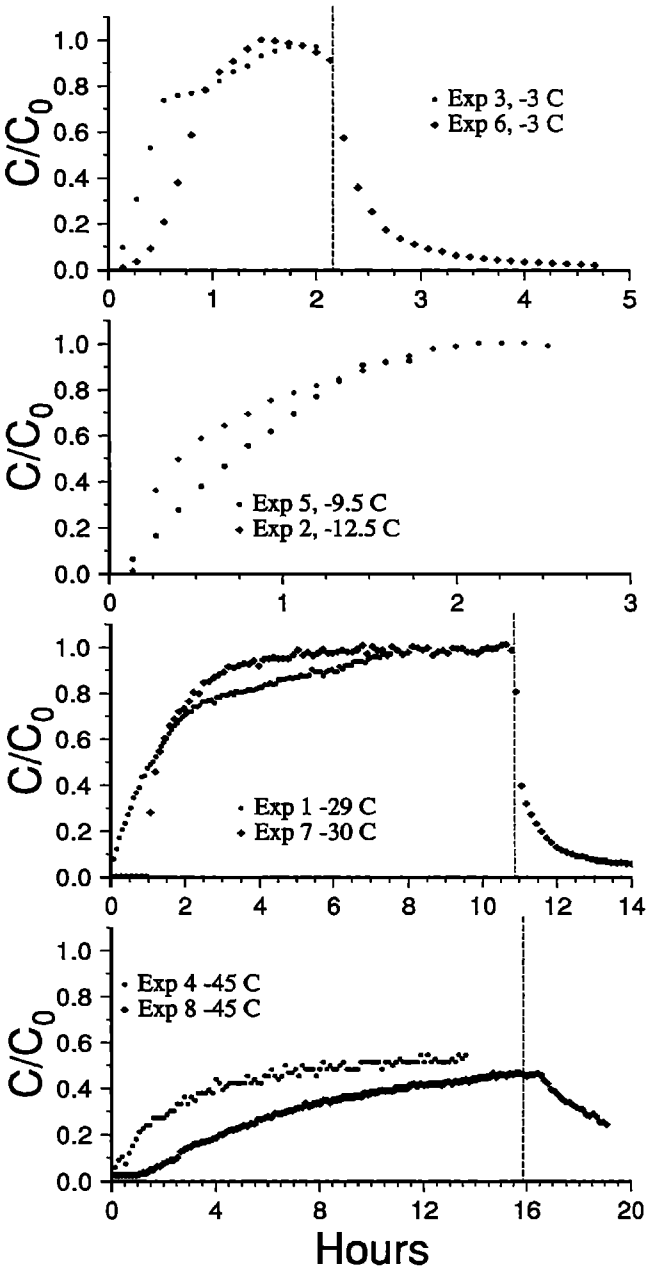

Fig. 3. Experimental results; conditions noted in Table 1.

in the equilibrium model. We thus estimate that P should be somewhat greater than these fitted values. To account for uncertainty in our estimate of P, we used three different (fixed) P values (100, 20, 10) in making estimates of the remaining first-order model parameters R and ω. Note that the dispersion Peclet number should be insensitive to temperature, so common values were used for all experiments.

Fitted parameters (ω and R) for all three Peclet numbers were within 10% of each other, well within the standard error of the estimate; only those for $P = 20$ are given in Table 2. An independent measurement of R was obtained by integrating the areas above the breakthrough curves. This area represents the fraction of H_2O_2 passing into the column that accumulated on the ice. Fitted R values were within 15% of those measured. Fitting the two breakthrough curves at each temperature together gives a clearer pattern of the parameter estimates (Figure 4 and Table 3). Accumulation

TABLE 2. Parameters Estimated From Model Fits of Each Experiment

		Area	Equilibrium Model Fits[a]			First-Order Model Fit		
Exp	Temperatures, °C	$10^{-3}R$	$10^{-3}R$	P	ssq[b]	$10^{-3}R$	ω	ssq[b]
1	-29	606	283 ± 6	0.77 ± 0.04	0.0346	556 ± 11	2.2 ± 0.1	0.2349
2	-12.5	101	62 ± 4	1.5 ± 0.2	0.0280	94 ± 4	2.9 ± 0.5	0.0496
3	-3	89	–[c]	–[c]	0.6436	103 ± 20	2.2 ± 1.3	0.6560
4	-45	–[d]	–[d]	–[d]	...	5,640 ± 210	1.5 ± 0.05	0.2622
5	-9.5	112	89 ± 4	2.5 ± 0.4	0.0184	111 ± 1	4.8 ± 0.3	0.0044
6	-3	108	104 ± 1	14.2 ± 1.5	0.0066	105 ± 1	47 ± 12	0.0041
7	-30	630	499 ± 10	6.2 ± 0.7	0.1456	529 ± 10	14.1 ± 2.6	0.1935
8	-45	–[d]	–[d]	–[d]	...	6,630 ± 140	3.1 ± 0.1	0.1901

[a]Fit ± std. error; for experiments 6-8, fit is for sorptions portion of curve.
[b]Sum of squared errors.
[c]Fit not statistically significant.
[d]Not determined due to incomplete breakthrough.

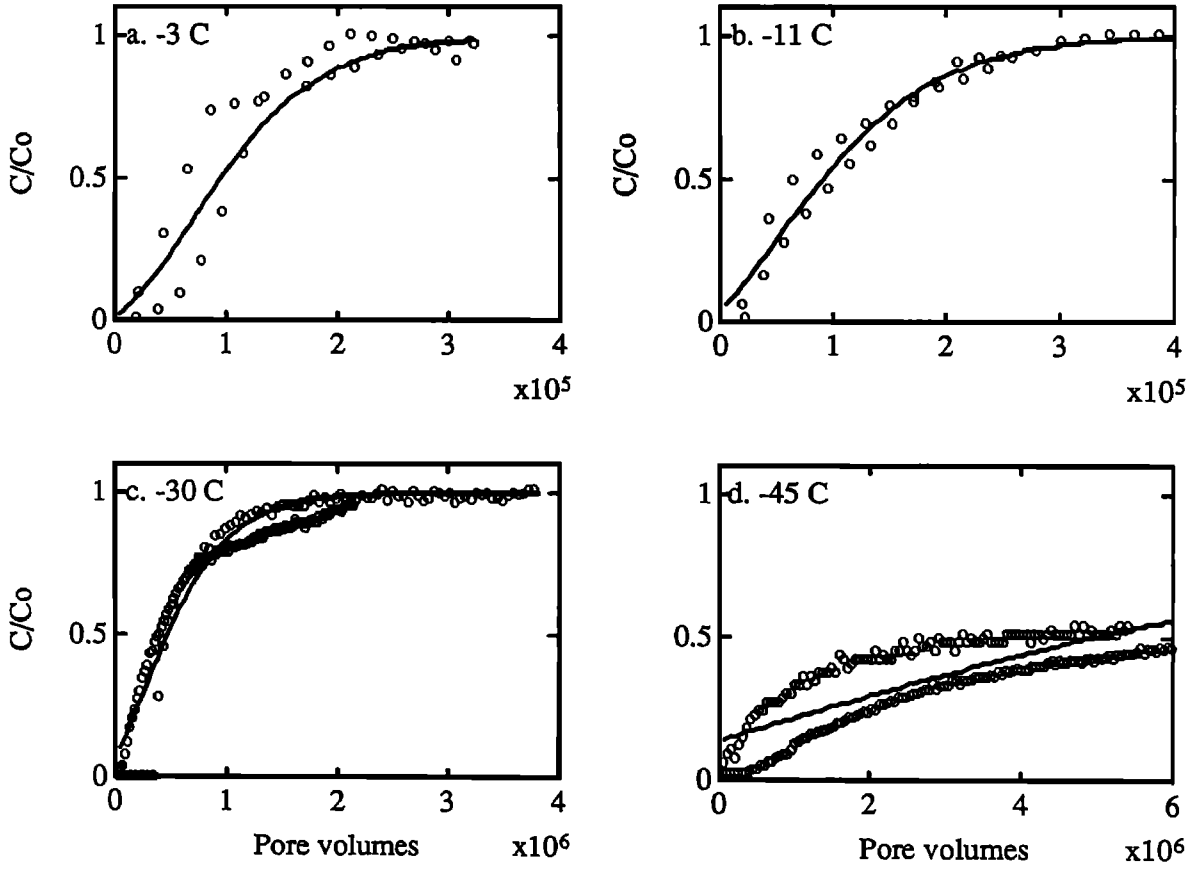

Fig. 4. First-order model fits to experimental data; parameters for fitted curves are in Table 3.

of H_2O_2 in the ice was relatively insensitive to temperature down to -12.5°C, but increased significantly below that temperature. The ω values were in the range of 2-5 for most experiments, indicating nonequilibrium processes were important for all temperatures.

DISCUSSION

H_2O_2 uptake in our experiments is thought to be influenced by deposition and redistribution processes, as well as adsorption and phase partitioning. In particular, ice surface area decreased over the course of the experiment due to sintering of the spheres. This caused local oversaturation conditions at grain junctions or necks, as described by the Kelvin equation [*Hobbs*, 1974]. This was greatest for newly packed columns, where the curvature of the concave surface is greatest. Because the ice spheres in the column were aged only between 4 and 36 hours (that is, newly packed columns) prior to an experiment, an enhanced water molecule transport due to evaporation from concave surfaces with smaller-neck radii and recondensation on surfaces with larger radii should occur. Measurements of the fraction of water molecules involved in this process by diffusion, as a function of temperature and sphere radius, have been made by *Hobbs and Mason* [1964] for ice spheres in a quiescent condition with no thermal gradients. A rough estimation indicates that up to 1% of the H_2O molecules could be redistributed under our experimental conditions, especially at the higher temperatures.

TABLE 3. Parameters Estimated From Fitting Combined Experimental Data[a]

Average Temperature, °C	10^{-3} R	ω	ssq[b]	K_D, $cm_a^3\,cm_i^{-3}$	k_f, s^{-1}	α	D_i, $m^2\,s^{-1}$
-3	103 ± 9	5.1 ± 2.1	0.920	83,000	210	0.018	4.4×10^{-14}
-11	103 ± 3	3.6 ± 0.4	0.094	124,000	150	0.019	3.1×10^{-14}
-30	545 ± 11	3.1 ± 0.2	0.895	578,000	170	0.024	5.0×10^{-15}
-45	6410 ± 263	2.1 ± 0.1	1.72	10,700,000	230	0.022	2.9×10^{-16}

[a]Parameters determined by simultaneously analyzing both sets of data at each temperature.
[b]Sum of squared errors.

Local oversaturation of water vapor (see below) in the column might temporarily lead to an efficient uptake of H_2O_2 by codeposition of H_2O and H_2O_2, yielding H_2O_2 oversaturated "spots" in the column. However, the large uptake amounts and greater uptake at lower temperatures suggest that codeposition did not dominate the H_2O_2 uptake. For our experimental conditions the amount of codeposition depended on the age of column, with the primary effect being on the shape of the breakthrough curve (cf. observations of different shapes at the same temperature; Figure 3). Codeposition of H_2O_2 and H_2O molecules from the flowing gas stream must also be considered. Calculations of effective diffusion lengths for H_2O molecules for a 0.05-s time interval (column residence time for 5-cm columns) shows that each H_2O and H_2O_2 molecule introduced in the column should hit the snow surface at least once. Taking a diffusion length (l_D) to be $\sqrt{D_0 t}$ and $D_0 = 1.8 \times 10^{-5}\ m^2\,s^{-1}$ (diffusion coefficient of H_2O in air at 0°C [*Weltz et al.*, 1976]) gives l_D = 0.95 mm. This decreases to 0.79 mm for -45°C. It can also be noted that even for the lowest temperature (-45°C) advection in the column carried at least 10 times more water molecules than were moved by evaporation and recondensation processes. Hence advection should significantly accelerate the sintering processes and contribute to local H_2O_2 oversaturated "spots."

There is ample evidence from laboratory as well as field studies that the vapor deposition of H_2O_2 on ice occurs by cocondensation, that is, codeposition without fractionation, when snow grows in supersaturated air [*Jacob*, 1990; *Sigg*, 1990]. A recent field study [*Snider et al.*, 1992] suggests fractionation of H_2O_2 occurs on riming ice particles. This is attributed to losses that occur specifically in the riming process. Cocondensation implies the same accommodation (sticking) coefficient for H_2O and H_2O_2 molecules.

The hypothesis that no fractionation of H_2O_2 occurs during incorporation into ice surfaces can be tested by estimating the sticking coefficient (α) for H_2O_2; α can be calculated by comparing the removal on the breakthrough curve with the rate at which molecules are transported to the ice surfaces, that is from the fitted ω values. For $d = 200 \times 10^{-6}$ m, $D_0 = 0.2$ to $0.87 \times 10^{-5}\ m^2\,s^{-1}$ for 0°C to -45°C, respectively [*Hirschfelder et al.*, 1964] and other parameters given in Tables 1 and 2, values of α are on the order of 0.02 (Table 3).

Continuous records of the water isotopes and the H_2O_2 concentration in polar ice cores show a damping of the initial seasonality due to redistribution processes on longer time scales. These processes can be quantitatively described by a displacement length integrated over the whole firnification process. Analysis of high-accumulation cores suggests a 50% larger displacement length for H_2O_2 molecules than for water molecules [*Johnsen*, 1977; *Sigg*, 1990]. From this, one can conclude that the accommodation coefficient of H_2O_2 molecules on ice surfaces in undersaturated or saturated conditions is smaller than for water, and is less than one, as estimated above. A trend of increasing mass accommodation coefficient with decreasing temperature was reported by *Worsnop et al.* [1989] for H_2O_2 on aqueous surfaces (for temperatures of -13° to 25°C). Their measured value for α, 0.2 at 0°C, was obtained for super-cooled droplets. They postulated a two-step process, with an initial physisorbed state that is a precursor to the final chemisorption, implying that the physisorbed H_2O_2 is relatively strongly bonded, however, there is a large orientation constraint limiting the penetration of H_2O_2 into the aqueous surface. This constraint might be higher for the more structured surface of ice. Another explanation is that the low sticking coefficient for our system may suggest that the slow mass transfer is due to additional processes, such as diffusion into the ice matrix.

On surfaces that are relatively stable, either adsorption or absorption processes can occur, depending on the properties of the ice surface. The structure and chemical reactivity of the disordered surface region at the ice-air interface are still under debate and investigation. The thickness of the surface-disordered layer decreases steeply with decreasing temperature, and is thought to not be important below -30°C [*Golecki and Jaccard*, 1978; *Gubler*, 1982]. Assuming their estimates of an equivalent thickness of 100 nm at -1°C, and 30 nm at -10°C and assuming that Henry's law applies to this bulk phase, gas/liquid partitioning can explain only up to 20% of the H_2O_2 uptake in the experiments with temperature $\geq$ -12.5°C; for the lower temperatures the fraction drops to less than 5%. *Conklin and Bales* [1993] report equivalent liquid fractions of the order of 0.0007 at −30°C to 0.007 at −1°C, inferred from SO_2 uptake on ice spheres like those used in the current experiments. Their numbers suggest that of the order of 15–50% of the observed H_2O_2 uptake could be attributed to gas/liquid partitioning, depending on temperature. The decrease in depth of disordered layer with decreasing temperature is opposite the trend in K_H. This suggests a change in mechanism as the temperature decreases, such as adsorption within ice-air interface rather than partitioning into the surface disordered layer.

Similar to the gas/liquid partitioning, adsorption at the ice-air interface should be a relatively fast process. For the 0.05-m column, a monolayer amounts to 50×10^{-9} mol H_2O_2; for the 0.025-m column, to 30×10^{-9} mol. The amount of H_2O_2 molecules taken up in the experiments exceeds a monolayer adsorption in the -29° and -45°C experiments run at the higher concentrations (7 and 8). Either multilayer adsorption, codeposition, or diffusion into the bulk ice is then required to explain the observed mass

sorbed. Certainly, the observation that some of the H_2O_2 is reversibly sorbed (as shown by the desorption curves) suggests that surface processes are important, but the slow desorption process may also suggest that the bulk ice is involved.

Time constants estimated from the experiments suggest that slow processes dominate the uptake or release of H_2O_2 by ice. Our alternative explanation, spherical diffusion, takes into account a mass transfer from air into the ice. When partitioning into ice is the rate-limiting step, the fitted dimensionless mass transfer coefficient (ω) is related to the product of the diffusion coefficient in ice (D_i) times the partitioning coefficient (K_D). Estimated values from our experiments for D_i are in the range of 3×10^{-16} to 4×10^{-14} $m^2 s^{-1}$ (for -60° to -3°C, respectively, see Table 3), which are in the same range as the estimated self-diffusion coefficient for H_2O in ice [*Hobbs*, 1974]. These values of D_i correspond to characteristic times, τ, of 40 days to 7 hours, respectively, where τ is defined as the time it takes for H_2O_2 to diffuse throughout the entire ice sphere and achieve a uniform concentration [*Seinfeld*, 1986]. These slow times suggest that the observed slow mass transfer involves bulk phase processes.

Neither the diffusion coefficient nor partitioning coefficients for H_2O_2 in ice at temperatures below 0°C have been measured. The H_2O_2 partition coefficient $\bar{C}_i/\bar{C}_a$ has been measured for pure single crystals only at 0°C [*Sigg et al.*, 1987]. The measured partitioning coefficient at 0°C, 0.014, is an estimate for the uptake capacity of the ice matrix for H_2O_2 molecules (this does not include grain boundaries and junctions). Incorporation of H_2O_2 in the ice lattice structure implies creation of defects. The probability of creating such defects decreases with decreasing temperature. Therefore, the H_2O_2 uptake under quasi-equilibrium conditions is also expected to decrease with decreasing temperature. Using a Henry's coefficient (K_H) of 8.92×10^4 mol L^{-1} atm^{-1} at 25°C and assuming a constant $\Delta H°$ of -55 kJ mol^{-1} [*Lind and Kok*, 1986], and using the van't Hoff equation [*Adamson*, 1975], one estimates K_H of 6.8×10^5 and 8.19×10^7 mol L^{-1} atm^{-1} at 0° and -45°C, respectively. Our estimated K_D values are roughly 0.4-0.6% of the Henry's coefficient extrapolated to the experimental temperatures. Neglecting surface accumulation, this implies a value of 0.004 to 0.006 for the water-to-ice partition coefficient, about one-third of the value measured by *Sigg et al.* [1987].

Figure 5 shows the temperature dependence of the different transfer functions: (1) pure air-liquid solubility given by the Henry's coefficient extrapolated to temperatures below 0°C; (2) codeposition of H_2O_2 and H_2O in the same molar ratios; and (3) experimentally determined K_D values. It is interesting that the trend of less uptake with increasing temperature from −45° to −11°C parallels both the Henry's law and codeposition curves. If Henry's law controlled uptake, the curves should come closer together at higher temperatures; the increase in fraction of liquid water for gas uptake should more than offset the decrease in K_H as temperatures approach 0°C [*Conklin and Bales*, 1993]. The circled region in Figure 5 represents the ratio of measured atmospheric concentration to snow concentrations measured at Summit, Greenland (data from *Sigg et al.* [1992*b*]).

It is somewhat surprising that codeposition gives a value for the transfer function that is only 2–6 times our laboratory results. Comparing these two curves gives an upper estimate for a sticking coefficient, the ratio of experimental values to codeposition, giving a value of 0.2 for -45° ≤ T ≤ -11.5°C, which is close to the measured value of *Worsnop et al.* [1989]. At -3°C, the experimental value approaches the codeposition curve, giving an α of 0.5. This estimate of α assumes a sticking coefficient of 1 for water. Since codeposition involves mainly the surface region of grains, the ice-air interface, this transfer function needs to reflect the extent of water-molecule deposition and redistribution. Further redistribution into the bulk ice would involve either solid-phase diffusion or significant redistribution of water molecules, that is, metamorphism of the ice. Codeposition must also take the possible differences in α for H_2O and H_2O_2 into account. Since uptake into the bulk phase is thought to be important, cocondensation might provide the upper limit for the partition coefficient between air and ice.

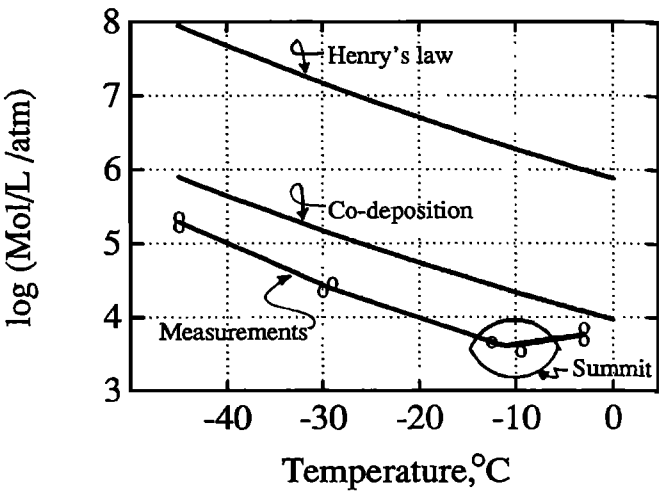

Fig. 5. Comparison of various equilibrium transfer functions with experimental data. Measurements are from the current experiments. The area marked "Summit" reflects conditions in Greenland.

The data show a trend of less uptake with increasing temperature from −45° to −11°C, but the uptake at −3° is essentially the same as at −11°C. This transition in behavior could reflect a change in the liquid properties of the ice surface in that temperature region, as observed with SO_2 uptake [*Conklin et al.*, 1993] and NO [*Sommerfeld et al.*, 1992].

CONCLUSIONS

Our experiments clearly show that the uptake of H_2O_2 on ice is reversible. In addition, our results demonstrate that uptake is greater at colder temperatures. At a given temperature, equilibrium uptake of H_2O_2 by ice was proportional to gas-phase concentration. Together, these imply that changes in both atmospheric concentration and ambient temperature induce changes in H_2O_2 concentrations in snow and firn.

Our estimates of time scales over which this reversible exchange range from hours at -3° and -11°C to weeks at -30° and -60°C. That is, one can expect diurnal changes in H_2O_2 in polar surface snow during the summer time and seasonal changes in H_2O_2 in snow during the colder winter. At all temperatures studied, bulk-phase partitioning of H_2O_2 in ice apparently controls the rate of exchange.

We made two estimates for the sticking coefficient for H_2O_2 to the ice surface. First, our observed uptake at -11°C and below was about 20% of the amount that would occur with cocondensation. Assuming a sticking coefficient

of 1.0 for H_2O, this implies a sticking coefficient of 0.2 for H_2O_2. At -3°C, the ratio was about 0.5. A sticking coefficient in the range of 0.2-0.5 does support the suggestion that H_2O_2 has a longer diffusion length in firn than does $\delta^{18}O$ [*Sigg et al.*, 1992*b*]. Second, we estimated a sticking coefficient of about 0.02 from the advection-dispersion model. This latter estimate was influenced by the slow bulk-phase diffusion into ice, however, and is probably a lower estimate for α.

Our results point to some of the key processes that need to be verified in the field. In the days to weeks after H_2O_2 is deposited, concentrations in the snow should change in response to changing atmospheric conditions. Both redistribution within the snow as well as uptake to or degassing from the near-surface snow should occur. Concurrent measurements of temperature, gas phase H_2O_2 concentration and H_2O_2 concentration in the snow, with depth, are needed to detect changes in the snow/firn column. Gas-phase measurements should be made directly above the snow surface to look for degassing of H_2O_2 from the snow during the cold, dark conditions that occur during the winter half of the year.

NOTATION

A_s factor relating single sphere collector to an assembly of packed spheres.

$\bar{C}_a$ time and spatial average atmospheric concentration in atmosphere.

$\bar{C}_i$ mean ice concentration over a specific depth interval.

C_0 initial concentration in air, mol m^{-3}.

C_1 dimensionless air concentration.

C_2 dimensionless ice concentration.

C_3 dimensionless ice concentration at any point in a sphere.

C_a air concentration, mol m^{-3}.

C_{ad} air-ice interface concentration, mol m^{-2}.

C_b bulk ice concentration, mol m^{-3}.

C_i ice concentration, mol m^{-3}.

C_r local ice concentration at any point in a sphere.

C_s surface-disordered layer concentration, mol m^{-3}.

D_a dispersion coefficient in flowing air, m s^{-1}.

D_i diffusion coefficient in ice.

D_0 diffusion coefficient in air.

K_D air-to-ice equilibrium partition coefficient, $cm_a^3\ cm_i^{-3}$.

K_H Henry's coefficient, mol L^{-1} atm^{-1}.

L column length, m.

P Peclet number.

Pe diffusion Peclet number.

R retardation factor.

T dimensionless time.

X dimensionless column distance.

a average ice sphere radius, m.

d ice sphere diameter, m.

k_b pseudo-first-order reverse rate coefficient or mass transfer coefficient, s^{-1}.

k_f pseudo-first-order forward rate coefficient or mass transfer coefficient, s^{-1}.

l_D diffusion length, m.

r radial distance, m.

t time, s.

u_a linear velocity, m s^{-1}.

x distance, m.

α sticking coefficient.

β R^{-1}.

γ dimensionless parameter in spherical diffusion equation.

ε $\theta_a^{1/3}$.

η single collector removal efficiency.

ξ dimensionless radial distance.

θ_a volume fraction of air.

θ_i volume fraction of ice.

τ time for H_2O_2 to diffuse throughout entire ice sphere.

ω Damkohler number.

Acknowledgments. The research was supported in part by National Science Foundation (NSF) grant DPP-9123025 to the University of Arizona (UA). The experimental apparatus was constructed and preliminary work done as part of NSF grant ATM-8909460 to UA. Support to initiate the experiments was provided by the UA's Coordinating Committee on Global change. T. Corley assisted with all aspects of the experiments, H. Unland helped with data analysis, and R. Brice did the manuscript preparation. Review comments by T. Staffelbach were extremely helpful in improving this manuscript.

REFERENCES

Adamson, A. W., *A Textbook of Physical Chemistry*, Academic, San Diego, Calif., 1975.

Conklin, M. H., and R. C. Bales, SO_2 uptake on ice spheres: liquid nature of ice-air interface, *J. of Geophys. Res.*, in press, 1993.

Conklin, M. H., R. A. Sommerfeld, K. Laird, and J. E. Villinski, Sulfur dioxide reactions on ice surfaces: Implications for dry deposition to snow, *Atmos. Environ.*, *27A*, 159–167, 1993.

Dasgupta, P. K., S. Dong, H. Hwang, H. C. Yang, and Z. Genfa, Continuous liquid-phase fluorometry coupled to a diffusion scrubber for the real-time determination of atmospheric formaldehyde, hydrogen peroxide and sulfur dioxide, *Atmos. Environ.*, *22*, 949–963, 1988.

Friedlander, S. K., Theory of aerosol filtration, *Indust. Eng. Chem.*, *50*, 1161–1164, 1958.

Golecki, I., and C. Jaccard, Intrinsic surface disorder in ice near the melting point, *J. Phys., C: Solid State Phys.*, *11*, 4229–4237, 1978.

Gubler, H., Strength of bonds between ice grains after short contact times, *J. Glaciol.*, *28*, 457–473, 1982.

Gunz, D. W., and M. R. Hoffmann, Field investigation on the snow chemistry in central and southern California, I, inorganic ions and hydrogen peroxide, *Atmos. Environ.*, *24A*, 1661–1671, 1990.

Happel, J., Viscous flow in multiparticle systems: slow motion of fluids relative to beds of spherical particles, *Am. Inst. of Chem. Eng. J.*, *4*, 197–201, 1958.

Hirschfelder, J. O., C. F. Curtiss, and R. B. Bird, *Molecular Theory of Gases and Liquids*, John Wiley, New York, 1964.

Hobbs, P., *Ice Physics*, Clarendon, Oxford, 1974.

Hobbs, P. V., and B. J. Mason, The sintering and adhesion of ice, *Philos. Mag.*, *9*, 181–197, 1964.

Hwang, H., and P. K. Dasgupta, Fluorometric flow injection determination of aqueous peroxides at nanomolar level using membrane reactors, *Anal. Chem.*, *58*, 1521–5124, 1986.

Jacob, P., Wasserstoffperoxid in der atmospharischen Gas- und Flussigphasenchemie: Laborstudien und Felduntersuchungen, Ph.D. thesis, University of Dortmund, Dortmund, Germany, 1990.

Johnsen, S. J., Stable isotope profiles compared with temperature profiles in firn with historical temperature records, in Proceedings of the Grenoble Symposium, August/September 1975, *IAHS Publ., 118*, pp. 388-392, 1977.

Levich, V. G., *Physicochemical Hydrodynamics*, pp. 80–87, Prentice-Hall, Englewood Cliffs, NJ, 1962.

Lind, J. A., and G. L. Kok, Henry's law determinations of aqueous solutions of hydrogen peroxide, methylperoxide, and peroxyacetic acid, *J. Geophys. Res.*, *91*, 7889–7895, 1986.

Neftel, A., P. Jacob, and D. Klockow, Measurements of hydrogen peroxide in polar ice samples, *Nature*, *311*, 43–45, 1984.

Neftel, A., P. Jacob, and D. Klockow, Long-term record of H_2O_2 in polar ice cores, *Tellus*, *38B*, 262–270, 1986.

Perla, R., Temperature-gradient and equi-temperature metamorphism of dry snow, in *Comptes Rendus*, paper presented at Second International Meeting on Snow and Avalanches, Association Nationale pour l'Etude de la Neige et des Avalanches, Grenoble, France, April 12-14, 1978.

Seinfeld, J. H., *Atmospheric Chemistry and Physics of Air Pollution*, John Wiley, New York, 1986.

Sigg, A., Wasserstoffperoxid-Messungen an Eisbohrkerner aus Gronland und der Antarktis und ihre atmospharenchemische Bedeutung, Ph.D. dissertation, 140 pp., Physikalisches Institut, Universität Bern, Bern, Switzerland, 1990.

Sigg, A., and A. Neftel, Seasonal variations in hydrogen peroxide in polar ice cores, *Ann. Glaciol.*, *10*, 157–162, 1988.

Sigg, A., and A. Neftel, Evidence for a 50% increase in H_2O_2 over the past 200 years from a Greenland ice core, *Nature*, *351*, 557–559, 1991.

Sigg, A., A. Neftel, and F. Zurcher, Chemical transformations in a snow cover at Weissfluchjoch, Switzerland, situated at 2500 m.a.s.l., in *Seasonal Snowcovers: Physics, Chemistry, Hydrology*, edited by H. G. Jones and W. J. Orville-Thomas, pp. 269-280, NATO Advanced Studies Institute, Reidel, Amsterdam, 1987.

Sigg, A., A. Neftel, and P. K. Dasgupta, A miniaturized, battery powered H_2O_2 monitor for airborne measurements in a motor glider, in *Air Pollution Research Report 41*, Commission of the European Communities, edited by I. Allegrini, pp. 111-117, Dordrecht, Boston, 1992*a*.

Sigg, A., T. Staffelbach, and A. Neftel, Gas phase measurements of hydrogen peroxide in Greenland and their meaning for the interpretation of H_2O_2 records in ice cores, *J. Atmos. Chem.*, *14*, 223–232, 1992*b*.

Snider, J. R., D. C. Montague, and G. Vali, Hydrogen peroxide retention in rime ice, *J. Geophys. Res.*, *97*, (D7), 7569–7578, 1992.

Sommerfeld, R. A., and T. L. Freeman, Making artificial snow for laboratory use, *USDA For. Serv. Res. Note RM-486*, 3 pp., 1988.

Sommerfeld, R. A., M. H. Conklin, and K. Laird, No adsorption on ice at low concentrations, *J. Colloid and Interface Sci.*, *149*, 569–574, 1992.

Van Genuchten, M. T., Non-equilibrium transport parameters from miscible displacement experiments, *Tech. Res. Rep. 119*, 88 pp., U.S. Salinity Laboratory, Riverside, Calif., 1981.

Van Genuchten, M. T., A general approach for modeling solute transport in structured soils, in *Hydrogeology of Rocks of Low Permeability, IAH Mem. 17*(2), 513–526, International Association of Hydrogeologists, Ottowa, Ont., 1985.

Van Genuchten, M. T., and P. J. Wierenga, Mass transfer studies in sorbing porous media, I, Analytical solutions, *J. Soil Sci. Soc. Am.*, *40*, 473–480, 1976.

Weltz, J. R., C. E. Wicks, and R. E. Wilson, *Fundamentals of Momentum, Heat, and Mass Transfer*, John Wiley, New York, 1976.

Worsnop, D. R., M. S. Zanhiser, M. S. Kolb, J. A. Gardner, L. R. Watson, J. M. V. Dover, J. T. Jayne, and P. Davidovits, The temperature dependence of mass accomodation of SO_2 and H_2O_2 on aqueous surfaces, *J. Phys. Chem.*, *93*, 1159-1172, 1989.

Zhang, L., P. K. Dasgupta, and A. Sigg, Determination of gaseous hydrogen peroxide at parts per trillion levels with a nafion membrane scrubber and a single-line flow-injection system, *Anal. Chim. Acta*, *260*, 57–64, 1992.

R. C. Bales and M. H. Conklin, Dept. of Hydrology and Water Resources, University of Arizona, Building 11, Tucson, Arizona 85721

A. Neftel and A. Sigg, Physics Institute, University of Bern, Sidlerstrasse 5, CH-3012 Bern, Switzerland

(Received August 14, 1992;
revised April 23, 1993;
accepted April 29, 1993.)